Robust Camera Calibration by Optimal Localization of Spatial Control Points

Jianyang Liu, Youfu Li, and Shengyong Chen, *Senior Member, IEEE*

***Abstract*— This paper proposes a novel method for localization optimization of control points for robust calibration of a pinhole model camera. Instead of performing accurate subpixel control point detection by specialized operators, which are normally adopted in conventional work, our proposed method concentrates on estimating the optimal control points in regions of plausibility determined by distortion bias from perspective distortion, lens distortion, and localization bias from out-of-focus blurring. With this method, the two main strict preconditions for camera calibration in conventional work are relieved. The first one is that the input images for calibration are assumed to be well focused and the second one is that the individual control point needs to be detected with high accuracy. In our work, we formulate the accurate determination of control points' localization as an optimization process. This optimization process takes determined control points' uncertainty area as input. A global searching algorithm combined with Levenberg–Marquardt optimization algorithm is introduced for searching the optimal control points and refining camera parameters. Experimental results show that the proposed method achieves higher accuracy than the conventional methods.**

***Index Terms*— 2-D control point localization optimization, camera calibration, out-of-focus blurring, perspective distortion, points' uncertainty area (PUA).**

I. Introduction

CAMERA calibration using a specified mathematical model with [1], [2], [4] or without considering lens distortion model [7], [8] is an essential step in the optical measurement. A number of methods have been investigated in this issue, which can be simply divided into three categories: 3-D reference-object-based calibration [1], 2-D planar-based calibration [2], [3], and self-calibration [9]. In the first category, a well-made 3-D calibration target with known geometry is needed to establish the 3-D points on the object and the corresponding 2-D image point on the image plane. The 2-D planar-based calibration method [2] requires a planar pattern with a few different orientations for camera calibration. Comparing with the 3-D reference-object-based method, it is more flexible. Moreover, the algorithm has been implemented in many software, such as MATLAB toolbox [10], OpenCV [11], and so on. The last category is usually called self-calibration method, which does not need any objects of specific known dimension, or even without any calibration objects. In this paper, our method falls into the second category, and we take the example on the traditional pinhole camera model.

In the process of pinhole model camera calibration, the 3-D object points are always assumed to project on the camera image plane through perspective transformation. The points on the image plane are called control points or feature points. Recently, the problem on how to accurately extract the control points received increasing interest. Pervious contributions [12], [13] showed that precise location of the control points in an image is extremely important for camera calibration. In this paper, the 2-D checkerboard pattern on a calibration target (LCD panel) is selected for verification. It is worth to note that, our algorithm implementation is not limited to the checkerboard pattern, the circle, or the ring pattern can also be adopted. Considering typical application cases, such as some 3-D shape measurement system [16]–[19] and robotic navigation [20], input images for calibration commonly have various degree of defocus blurring. Moreover, lens focalization in these kinds of system is a tedious work if a camera is not equipped with an autofocus device. Even if it could focus automatic, areas in the computed images still have various degree of defocus blurring, because some prime lenses have narrow depth of focus due to its big aperture. Thus, in the out-of-focus area of the input images, the conventional extraction methods of control points cannot be directly used any more. More recently, numbers of control points extraction methods [13], [14] have been improved and perspective distortion is considered combining with conventional extraction methods of control points to get more accurate localization of control points. However, all these methods normally assume that the input images captured by camera are in good focus. To the best of our knowledge, little work is done in considering out-of-focus blurring influence together with perspective distortion and lens distortion bias for pinhole camera calibration. The most-similar one to our work is [21]. However, they proposed a unified method that just added reprojection blur width error of control points into the conventional cost function of reprojection control point error for camera parameters estimation. Moreover, the quantitative result of calibration accuracy was not reported in their work. In this paper, we focus on obtaining the accurate 2-D control point localization under a small

Manuscript received December 12, 2013; revised March 2, 2014; accepted April 8, 2014. Date of publication May 14, 2014; date of current version November 6, 2014. This work was supported in part by the Research Grants Council of Hong Kong under Project CityU 118613, in part by the National Natural Science Foundation of China under Grant 61273286 and Grant 61325019, and in part by the Ministry of Science and Technology of China under Grant 2014DFH10110. The Associate Editor coordinating the review process was Dr. Amitava Chatterjee.

J. Liu and Y. Li are with the Department of Mechanical and Biomedical Engineering, City University of Hong Kong, Hong Kong (e-mail: manchestsc@gmail.com).

S. Chen is with the College of Computer Science, Zhejiang University of Technology, Hangzhou 310023, China.

Color versions of one or more of the figures in this paper are available online at http://ieeexplore.ieee.org.

Digital Object Identifier 10.1109/TIM.2014.2324792

amount out-of-focus blurring condition for camera calibration. When the images for calibration are captured with severe blurring, even we could get the accurate localization of 2-D control points, using these estimated control points to obtain the camera parameters (i.e., the focus length of the system) would become severe biased or even meaningless.

To handle the problem of how to accurate determine the localization of control points under a certain degree of defocus blurring, perspective distortion, and lens distortion, we propose a novel generic localization optimization method of 2-D control points for camera's parameters estimation. In this method, we first determine the points' uncertainty area (PUA) map for potential optimal 2-D control points which by considering localization bias stem from out-of-focus blurring, distortion bias from perspective transformation, and lens distortion. Then, an optimal 2-D control points searching algorithm together with Levenberg–Marquardt (L–M) optimization algorithm are developed to accurately obtain the optimal 2-D control points meanwhile refining the parameters of a general pinhole model camera. The rest of the paper is organized as follows. In Section II, we give a brief review of camera model and the pinhole camera model with lens distortion is adopted. Section III introduces the initial parameters estimation of a pinhole model camera using traditional methods and available software. Section IV presents the method of PUA determination by considering localization bias stem from out-of-focus blurring, distortion bias from perspective transformation, and lens distortion. Also in this section, we develop the 2-D optimal control points searching algorithm combined with the L–M optimization algorithm for accurate determine the spatial localization of control points meanwhile robustly refining the camera's parameters. A summary about the whole procedure of the proposed method is also given in the end of this section. Section V lists the evaluation methods of conventional camera calibration. In Section VI, experimental results that consider the hypothetic in-focus condition and under a certain different degree of defocus blurring situations are provided to verify the calibration accuracy, and we give some discussion in Section VII and conclude this paper in Section VIII.

II. Camera Model With Lens Distortion Brief Review

Camera calibration consists in the estimation of a mathematical model for an uncalibrated camera. Dating from 60s of the last century, numbers of mathematical models for camera have been presented. According to the optimization algorithm for obtaining the camera's parameters, these models can be roughly divided into three categories. The first model is based on conventional method in photogrammetry. Faig [6] presented a mathematical camera model for the imaging process. The model describes the constraint relationship between the image and the 3-D object space using at least 17 parameters for each image view. It is proved to be accurate in 3-D reconstruction task, but meanwhile, it requires specific professional camera. The second one is the famous direct linear transformations model (DLT) which was first presented in [7]. The parameters are obtained by solving linear equations. Then, the linear

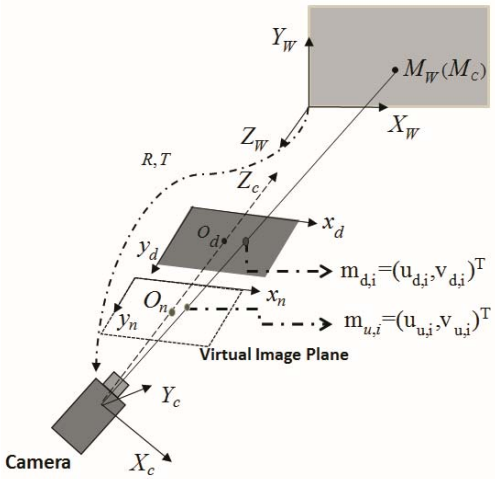

Fig. 1. Mathematical model of a camera.

model without considering lens distortion was proposed in [5]. The advantage of this method is the simplicity of the model that consists in a simple and rapid calibration. However, its drawback is that linear techniques are not accurate for lens distortion modeling and usually calibration result is rough. It is worthy noticing that an interesting variation of the DLT model is the double-plane based model, which is presented in [3]. This model involves two parallel control planes and is based on 2-D DLT model. The last one should be nonlinear models that consider the lens distortion. These are for more accurate for some applications where greater precision is needed. In general, a pinhole camera model is usually assumed in these nonlinear models at the first stage. Tsai's [1] well-known nonlinear model considering the radial lens distortion was proposed. In his work, a two-step technique is proposed. It first computes some of the parameters using a linear optimization algorithm, then in the second step, the rest of camera parameters are computed iteratively. Although all the parameters are iteratively optimized in the last step, the number of iterations is remarkably reduced using the calibrating algorithm proposed in this paper. Tsai's method makes use of the advantages of the previously methods, but it assumed that there are some camera parameters have been known from manufacturers. Zhang [2] reported a flexible planar-based calibration technique. This technique also first use a pinhole camera model to obtain the initial closed-form solution of intrinsic and extrinsic related matrix, then a two terms of radial distortion is added for further maximum likelihood estimation of refined parameters.

A. Idea Pinhole Camera Model

Without the loss of generality, the existing widely-used pinhole camera model presented in [2] is adopted in this paper. The projection transformation process from a 3-D point in space to a 2-D image point on the camera image plane is shown in Fig. 1.

The whole process can be described as follows.

1) Transformation From the 3-D World Reference Frame to the 3-D Camera Reference Frame:

$$M_c = RM_w + T \tag{1}$$

where $M_c = (X_c, Y_c, Z_c)^T$ and $M_w = (X_w, Y_w, Z_w)^T$ denote a 3-D point in the camera reference frame and the world reference frame, respectively. R is a 3×3 orthogonal rotation matrix and T is a 3×1 translation vector that represent the relative rotation and translation between the two reference frames, respectively.

2) Transformation From the 3-D Coordinate in Camera Reference Frame to the 2-D Normalized Image Coordinate:

$$m_n = (X_c/Z_c, Y_c/Z_c)^T. \tag{2}$$

3) Transformation From the 2-D Normalized Image Coordinate to the 2-D Undistorted Image Coordinate:

$$s\tilde{m}_u = A\tilde{m}_n \tag{3}$$

where A is the camera's intrinsic parameters matrix, s is a nonzero arbitrary scale factor, and $m_n = (x_n, y_n)^T$ is the previous normalized image point in unit metric. $\tilde{m}_u$ and $\tilde{m}_n$ is the homogeneous coordinates of m_u and m_n respectively. The intrinsic parameters matrix A is denoted as

$$A = \begin{bmatrix} f_x & \lambda & u_0 \\ 0 & f_y & v_0 \\ 0 & 0 & 1 \end{bmatrix} \tag{4}$$

where (u_0, v_0) is the coordinate of the principle point. f_x and f_y are the focal length in pixels of the camera image plane along u and v axes, λ denotes the skewness of the two image axes.

B. Lens Distortion Model

In general, the ideal pinhole model is an approximation of a real world projection process. Hence, the radial distortion and tangential distortion models are both considered in this paper. In addition, we use a distortion model up to fourth-order component in this paper. By considering the lens distortion, the nondistorted point $m_u(x_u, y_u)$ is replaced by the corrected normalized 2-D image point m_d, which can be described as follows:

$$m_d = (1 + k_1 r^2 + k_2 r^4)\begin{pmatrix} x_u \\ y_u \end{pmatrix} + \begin{bmatrix} 2k_3 x_u y_u + k_4(r^2 + 2x_u^2) \\ k_3(r^2 + 2y_u^2) + 2k_4 x_u y_u \end{bmatrix} \tag{5}$$

where $r = \sqrt{x_u^2 + y_u^2}$ and $k = (k_1, k_2, k_3, k_4, k_5)^T$ is a vector that contains both radial and tangential distortion coefficients.

III. Initial Camera Parameters Estimation Stage

A. Initial Localization of Control Points Estimation

In the last decade, several subpixel corner extraction algorithms have been implemented. The MATLAB toolbox [10] provided requires user to identify the four outbound corners of the checkerboard in each image by manually clicking on them. After that, the approximate locations of the corners include preclicked corner are estimated by a simply interpolation method and a Harris corner finder [15] and gradient-based approach searching is then employed to refine the corner to subpixel level. It is worthy noticing that Harris corner finder is not suitable anymore for corner extraction when the input images are captured under some degree of out-of-focusing. Similar to BouguetJY's toolbox, the algorithm presented in [22] and [23] is designed for fisheye and omnidirectional camera system calibration, respectively. In a fisheye or omnidirectional camera system, a checkerboard pattern imaged by either of them is severe blurred and distorted. Thus, it looks like the algorithm of corner extraction used in these two toolboxes can cope with the out-of-focus problem. However, we applied the corner extraction algorithm in these two toolboxes on the input images captured by a common camera (pinhole model) system, but the result is hardly satisfying. Hence, it is necessary to propose a new localization of spatial control point algorithm for handling out-of-focus blurring case. In the first initial camera's parameters estimation stage, a latest developed precise camera calibration algorithm presented in [24] is adopted to accomplish the task. Fig. 2 shows a sampled corner extraction result. It is worthy noticing that, the precise requirement for corner extraction algorithm is not so strict at this stage. For instance, any other corner extraction methods which satisfy the following demand are enough at this initial stage: 1) they can extract corners for captured out-of-focus blurred checkerboard pattern without ambiguity and 2) they can get subpixel level precision.

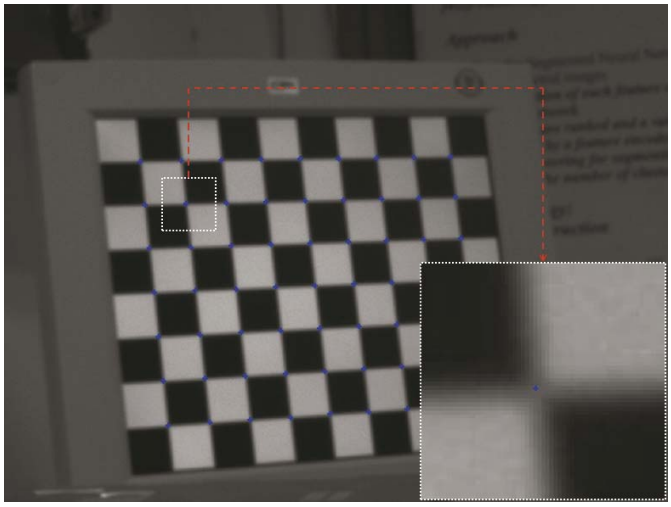

Fig. 2. Corner extraction result on a 10×8 checkerboard pattern image. One of the partial enlarged view of the extracted corner is on the bottom right of the figure, the blue cross indicates the extracted control point.

B. Initial Estimation of Camera Parameters

Given the estimated 2-D control points on each calibration plane with different orientation, the geometric relationship between the detected 2-D control points and their corresponding known 3-D control points can be obtained. The whole calibration process can be divided into two stages. First, a linear approximation is adopted to obtain an initial guess. Then, a L–M optimized algorithm is used to refine the initial guess of parameters iteratively. Generally, the global cost function may stuck in a local minimum caused by a high-order nonlinear lens distortion. However, the global optimal still can be reliably achieved by given a good initial input with the limited fourth-order distortion model. It is worth

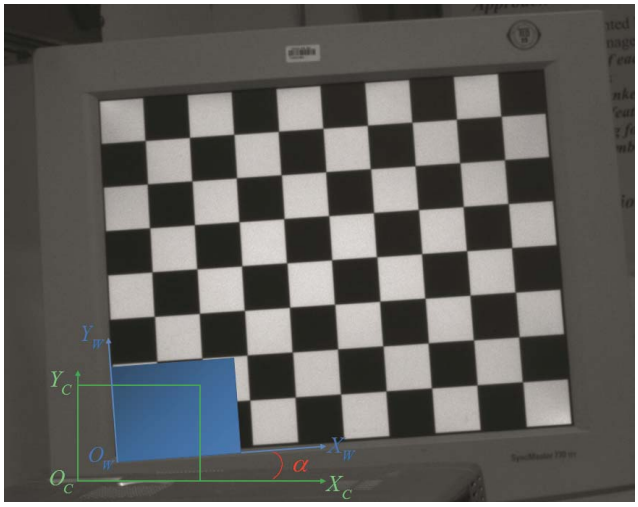

Fig. 3. Sample of nonfronto-parallel distorted image.

noticing that, after initialization calibration, each view with different orientation has different extrinsic parameters yet shares the same intrinsic parameters (R_i, T_i), as we mentioned in Section II-A. More details can be found in [2].

IV. Localization Optimization of Control Points

A. Perspective Distortion and Lens Distortion Bias Map Estimation

The main difficulty of obtaining accurate 2-D control points on calibration plane is directly dealing with the nonfronto-parallel distorted images (shown in Fig. 3). We can see from the figure that if the world coordinate system $(X_W O_W Y_W)$ is coplanar with the LCD panel plane, the image plane $(X_C O_C Y_C)$ forms an angle α with the LCD panel plane. Namely, we can say the bigger of the angle α, the more nonfronto-parallel image is distorted.

Hence, in this case, it is inherently biased to apply the corner extraction algorithm directly to determine the localization of control points [13]. Meanwhile, it is also difficult to distinguish the bias between the distortion from perspective effects and distortion from lens nonlinear distortion itself. To cope with such a problem, the intuitive method uses an iterative refinement approach for localizing the control points by iteratively undistorting and adjusting the input images to the canonical fronto-parallel image [as shown in Fig. 4(a)], which is then used to precisely localize the control points and reestimate the camera parameters. The whole procedure is performed in an iterative manner until convergence. However, as previously mentioned, these methods still assume the captured input images are well focused. Furthermore, the bias from perspective distortion and real lens nonlinear distortion has to be estimated and updated at each iterative process.

In this paper, we propose a more generic method to perform a once for all perspective distortion and lens distortion map estimation for each control point. Suppose we are given captured checkerboard images with different orientations that consist of numbers of target corners. The perspective distortion and lens distortion map is obtained using the following

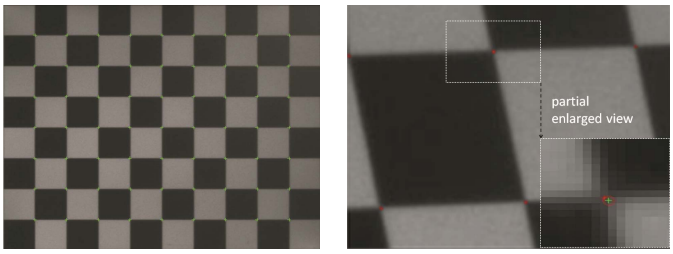

(a) (b)

Fig. 4. (a) Corrected canonical fronto-parallel image. (b) Partial view of perspective distortion and lens distortion bias map on input calibration image, one of enlarged view of perspective distortion, and lens distortion bias at the interest control point, the green cross indicates the initial extracted control point, the red circle denotes the estimated perspective distortion, and lens distortion bias area of this specific point.

steps. First, a specific method (i.e., Harris corner extraction algorithm) is adopted for the corner extraction task, and the corners' coordinates in its corresponding image coordinate system are initially obtained. After that, the initial camera parameters are estimated according to Section III-B. Thus, a reverse perspective distortion and lens distortion adjustment can be carried out to rectify the current nonfronto-parallel image to a canonical fronto-parallel one. Then the same corner extraction method is repeated to obtain the corners' coordinates on the canonical fronto-parallel one once again. The Euclidean distance in pixel between the corner point extracted at the first time and the second time is defined as perspective distortion and lens distortion bias. All the distortion bias corresponding to the original input image makes a bias map, which is shown in Fig. 4(b). A partial enlarged view of a sample control point in the perspective distortion map is also shown in the bottom right corner of Fig. 4(b).

B. Defocus Blurring Bias Map Estimation

We estimate the defocus blurring radius at each control point locations. Given a calibration target that is with a certain out-of-focus blurring, the light rays taht is reflected from the target and captured by the lens system (suppose it obeys the thin lens model) cannot converge into a single point. Instead, they are distributed in a small area (Fig. 5), which are usually called circle-of-confusion (COC). The diameter c of COC can be written as follows [25]:

$$c = \frac{|d - d_f|}{d} \frac{f_0}{D(d_f - f_0)} \tag{6}$$

where f_0 and D are the focal length and the aperture of the camera, respectively. d and d_f are the distance from the object plane to the lens plane and the focal plane to lens plane in a fixed lens system, respectively.

The defocus blurring radius of an image depends on both the size of the COC as well as the light distribution profile within it. In addition, the light distribution profile is typically called point-spread-function (PSF). In general, the imaging intensity of an object can be treated as a convolution of the true object and the PSF [26]. The PSF is determined by many factors such as aperture size and other nonlinear characteristics. The ideal pinhole model assumes an infinite depth of

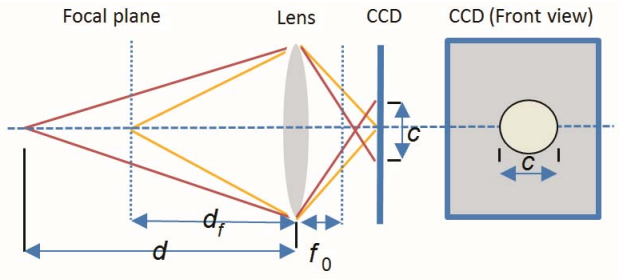

Fig. 5. Focus and defocus phenomenon in a camera with thin lens model.

field (DOF), which does not exist in practice. Therefore, the camera has to be refined into focus during the imaging process. Actually, the defocus problem still exists because the aperture of camera cannot be made infinite small. The PSF can be modeled as a 2-D circular Gaussian form [26]

$$G(x, y, \delta) = \frac{1}{2\pi\delta^2} \exp\left(-\frac{x^2 + y^2}{2\delta^2}\right) \tag{7}$$

where $\delta = \kappa c$ denotes the standard deviation of the Gaussian distribution and it determines the blurring radius or blurring degree. The intensity of the defocus image can be expressed as the result of a convolution

$$I_b(x, y) = \alpha I_u(x, y) \otimes G(x, y) \tag{8}$$

where $\otimes$ denotes the convolution operator, $\alpha \in [0, 1]$ is the reflectivity of a target object. I_u and I_b is the nonblurred images and the captured blurred images, respectively. It is worthy noticing that the inaccurate target is one of the main reasons for calibration precision degenerate [27]. Thus, the checkerboard pattern displaying on calibration plane (LCD panel) with different orientations is adopted in our paper. Compared with printed checkerboard on a paper, LCD panel's planarity is of industrial grade and is thus far more dependable, even consumer-level LCD panels have the assurance that the substrate glass surface of the panel has a planarity deviation of no more than 0.05 um [28]. Therefore, the corners of checkerboard pattern are the target control points to be optimized and all the control points can be regarded as ideally coplanar in real world coordinate system. Furthermore, the dimension of every pixel on LCD panel is precisely known, so we can obtain the real scale length of arbitrary point pair easily, which will also be used as ground truth in the latter experiments. Suppose the blurring radius of different control points on each calibration plane are not the same because of the limited DOF of camera. In this case, we should analyze the blur radius map for all the control points on the captured image. Blur radius estimation method from [25] is adopted in this paper. For convenience, we first derive the blurring radius along one axis of orientation, then, extend it to the practical 2-D case.

When the LCD panel is switched off, the captured image [Fig. 6 (a)] can be represented as

$$I_0(x) = (A + n(x)) \otimes G(x, \delta_x). \tag{9}$$

The image has an unknown offset A, which is actually the amount of reflection property of the LCD panel's surface with

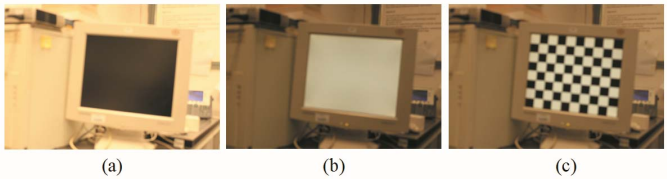

Fig. 6. LCD panel displaying different patterns. (a) Displaying a black pattern. (b) Displaying a white pattern. (c) Displaying a checkerboard pattern.

ambient light illumination. In addition, the noise $n(x)$, which is modeled as a stationary, additive, and zero-mean white noise, is added to this reference image.

Then, the LCD panel is turned ON with a white pattern [Fig. 6(b)], the captured image is assumed to be equal to the summation of the value from previous state (LCD panel is OFF) and background light illumination with unknown amplitude B, which is from the intensity of LCD panel's illumination itself. Thus, the intensity of the image can be denoted as

$$I_1(x) = (B + A + n(x)) \otimes G(x, \delta_x). \tag{10}$$

Finally, the LCD panel is turned ON with a checkerboard pattern [Fig. 6(c)], the captured image is clearly blurred because the aperture of the camera cannot be infinite small and DOF of the camera is limited. The blurred edge can be modeled as the summation of the first state (LCD panel is OFF) and the real-object's intensity

$$I_b(x) = (I_u(x) + A + n(x)) \otimes G(x, \delta_x). \tag{11}$$

To remove the influence of noise and reflectivity of the LCD panel's surface, the blurred image can be normalized as follows according to (9)–(11):

$$I_{nb}(x) = \left(\frac{I_b(x) - I_0(x)}{I_1(x) - I_0(x)}\right) \otimes G(x, \delta) = \frac{I_u(x)}{B} \otimes G(x, \delta_x). \tag{12}$$

The gradient of reblurred image is denoted as

$$\nabla I'_{nb}(x) = \nabla(I_{nb}(x) \otimes G(x, \delta_0)) \tag{13}$$

where ∇ denotes the gradient operator. δ_0 is the know standard deviation of Gaussian kernel.

Combining (12) and (13), we have the following equation:

$$\nabla I'_{nb}(x) = \frac{\nabla I_u(x)}{B} \otimes G\left(x, \sqrt{\delta_x^2 + \delta_0^2}\right). \tag{14}$$

Normally, the edge of the checkerboard pattern in-focus is assumed as a step-edge. The magnitude of gradient ratio between the first blurred image and the reblurred image can be described as

$$\left|\frac{\nabla I'_{nb}(x)}{\nabla I_{nb}(x)}\right|_{x=0} = \sqrt{\frac{\delta_x^2}{\delta_x^2 + \delta_0^2}}. \tag{15}$$

Assuming the magnitude along with x-axis is denoted by $1/R_x$

$$\frac{1}{R_x} = \sqrt{\frac{\delta_x^2}{\delta_x^2 + \delta_0^2}}. \tag{16}$$

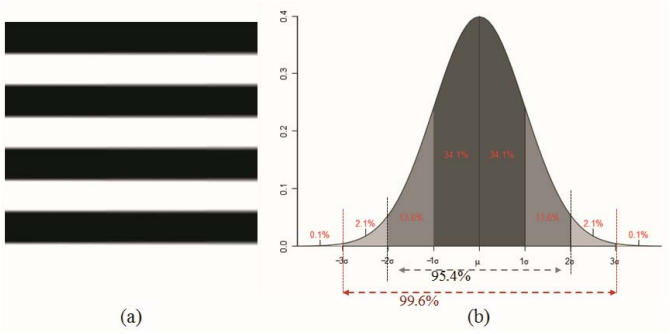

Fig. 7. (a) Synthetic image is blurred with increasing blur radius from 5.2 to 10, from left to right. (b) Standard deviation diagram for a Gaussian distribution.

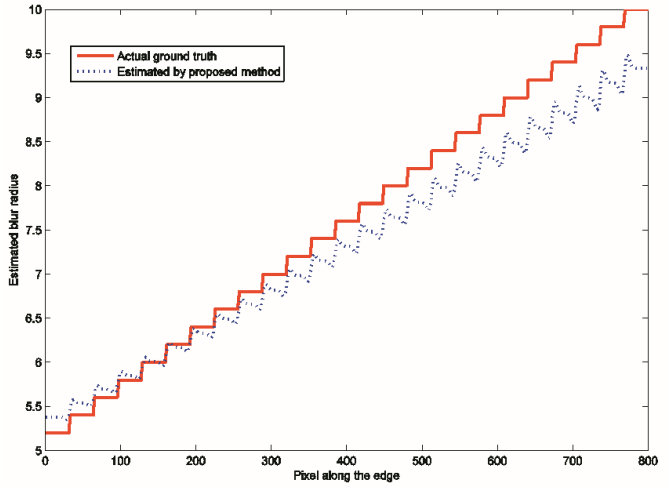

Fig. 8. Estimated blur radius (blue color line) and the actual blurring radius (red color line) along the edge using proposed method.

Thus, given the magnitude of the gradient ratio, the blur radius along x-axis can be obtained as

$$\delta_x = \frac{1}{\sqrt{R_x^2 - 1}}\delta_0. \tag{17}$$

In (17), it is worth noticing that the estimated blur radius is not affected by the unknown offset A and the edge amplitude B, which represent the ambient light reflection property and illumination intensity of object itself, respectively. Hence, in the practical 2-D case, the blurring estimation is a similar process and the magnitude of gradient in 2-D space can be written as

$$\nabla I'_{nb}(x, y) = \sqrt{\nabla^2 I_{nb}(x) + \nabla^2 I_{nb}(y)} \otimes G(x, y, \delta_0) \tag{18}$$

where $\nabla I_{nb}(x)_{and}$ $\nabla I_{nb}(y)$ are the gradients along x- and y-directions, respectively. To simply verify the algorithm performance for blur radius estimation, we synthesize a horizontal stripe image, which is shown in Fig. 7(a). The blur radius amount of the edge increases linearly in stepped appearance from 5.2 to 10. Fig. 8 shows that the result that indicates the method from [25] can handle this problem well.

In this paper, we set the blur radius double the estimated standard deviation of the Gaussian distribution. Because from the view of statistics, according to the three-sigma rule or empirical rule, the values which lie within triple deviations of the mean in the Gaussian distribution covers over 99% of whole distribution [as Fig. 7(b) shows]. However, in practical for our case, we find double deviation of blurring radius is enough for PUA estimation, which contains most possible potential control points. This will be discussed and verified by the experiment in Section VI. Fig. 9 shows the real blur radius estimation result of one of the practical input images for calibration. The radius red circle represents the blurring degree.

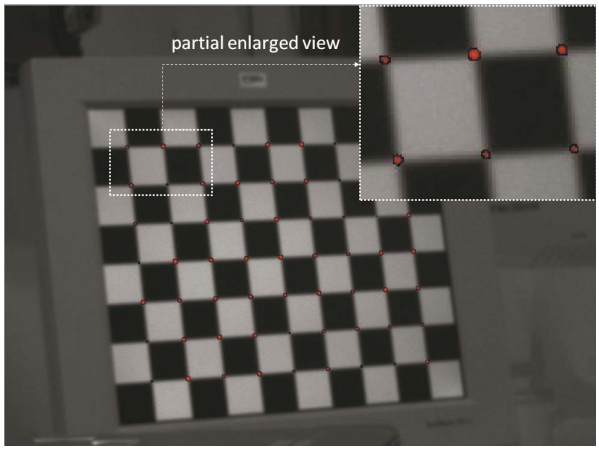

Fig. 9. Holistic estimated defocus blurring radius map, the red circle denotes the defocus blurring radius, and the image in the top-right corner is the partial enlarged view of the estimated defocus blur radius map.

C. Control PUA Map Determination

Although the control points are extracted at subpixel level in the previous initial corner extraction process, the inherent biases of corner localization still exists due to the defocus blurring influence, perspective distortion, and lens nonlinear distortion. The biases, although small, have a significant effect on the estimated camera parameters [13], [27]. Hence, the localization of extracted control points still has to be refined for camera parameters determination. To overcome this kind of problem in a more generic way, we propose to estimate control PUA map for refining the optimal control points. Similarly like the intuitive method in [29], the control PUA is defined as a circle-like area that takes the initial refined control point through perspective distortion and lens distortion adjustment as the circle center and the perspective distortion and lens distortion radius (γ), as the circle radius. Hence, it can be denoted as

$$\bar{D}_{ij,1} = \{(i, \gamma_i) | i \in N_j\} \tag{19}$$

where N_j is the jth input image for calibration, $\bar{D}_{ij,1}$ is one of the control PUA for perspective distortion bias and lens distortion bias. i is the index number of control point in each input image. Similarly, the second uncertainty area can be described using defocus blur radius (δ), as the circle radius, the initial estimated control point as the circle center. Let's denote it as

$$\bar{D}_{ij,2} = \{(i, \delta_i) | i \in N_j\} \tag{20}$$

where N_j is the jth input image for calibration, $\bar{D}_{ij,2}$ is one of the control PUA for defocus blurring radius. i is the index

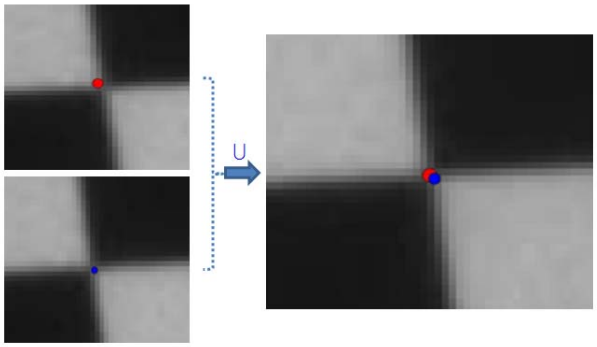

Fig. 10. Uncertainty area determination scheme of a sample control point, the red solid circle denotes the uncertainty area from defocus blurring and the blue solid circle implies the uncertainty area from perspective distortion and lens distortion.

number of control point in each input image. Combine the uncertainty area $\bar{D}_{ij,1}$ and the uncertainty area $\bar{D}_{ij,2}$, we get the final control PUA, which is denoted as

$$\text{PUA} = \left\{ m_{i,j} \left| m_{i,j} \in \bar{D}_{ij}, \bar{D}_{ij} = \bar{D}_{ij,1} \cup \bar{D}_{ij,2} \right. \right\} \tag{21}$$

where $\cup$ means getting the union uncertainty area between uncertainty area $\bar{D}_{ij,1}$ and uncertainty area $\bar{D}_{ij,2}$. Hence, the area for searching optimal control points can be restricted to a small region around the estimated coordinates, and this restriction reduces the searching computational time. The whole process can be described as shown in Fig. 10.

D. Localization Optimization of 2-D Control Points for Camera's Parameters Further Refinement

Given the PUA that contains potential target control points, the optimal solution of control points' localization can be obtained by utilizing a 2-D control points searching algorithm in PUA meanwhile with using L–M optimization algorithm to update and refine the camera's parameters by minimizing the cost function. Suppose, we are given n input images and each image has m control points data sets for searching, the cost function can be defined as follows:

$$\begin{aligned} F\left(m_{i,j}\right) &= \sum_{i=1}^{n} \sum_{j=1}^{m} \left\| m_{i,j} - \hat{m}(A, K, R_i, T_i, M_{i,j}) \right\|^2 \\ \text{s.t.} &\begin{cases} m_{i,j} \in PUA \\ \left\| M_{i,j} - M_{i+1,j} \right\| - D < \varepsilon \end{cases} \end{aligned} \tag{22}$$

where $m_{i,j}$ is the observed control point on the image plane. $M_{i,j}$ is the corresponding point of the observed control point on target plane in 3-D space. $\hat{m}(A, K, R_i, T_i, M_{i,j})$ is the reprojection point of 3-D position point $M_{i,j}$ on image plane according to (1)–(4), followed and refined by (5). PUA is the control, points including preestimated control point, potential optimal control point, and other uncertain control points. D is the real Euclidean distance, which is between the adjacent corner on the checkerboard pattern. ε is a given threshold value, it can be set depending on the required measurement accuracy. In this paper, we set $\varepsilon = 0.2$. It is obviously that the smaller value of it, higher measurement accuracy can be achieved, but meanwhile with more time-consuming. Similar to the cost function in [2], (22) is a constrained nonlinear minimization function. An initial localization guess of control points $m_{i,j}$ are obtained from the corner extraction process, as described in Section III-A. Meanwhile, an initial guess of A, K, R_i, T_i, M_j are given from the camera's initial calibration. In this paper, the target parameters are not only the parameters A, K, R_i, T_i, M_j, which are to be estimated, the final optimal control points $m_{i,j}$ are also the target parameter. It is worthy noticing that, this is different from the method used for minimizing the cost function in [2]. In our problem, we are given $n \times m$ control points to be refined. Even the 2-D searching area is restricted in obtained PUA, the searching dimension is still very large and the optimal control points searching for nonlinear cost function is very complicated. To alleviate the problem of searching results stuck into a local optimal solution, we explore a strategy based on genetic algorithms (GAs) and L–M optimization algorithm. The GAs is introduced to solve for this complicated problem because of it offers the good characteristic of efficiently searching a large, nonlinear spaces. It has been widely applied in solving difficult search and optimization problems including camera calibration [31], [32], instrument and model calibration [33], and other optimization problem [34]. In addition, the L–M optimization algorithm is adopted for seeking the minimum of cost function meanwhile updating the camera's parameters. Hence, by performing numbers of 2-D searching in the obtained PUA with a minimum value of cost function $(F\left(m_{i,j}\right)_{\min})$ under additional constraint, the optimal 2-D control points are obtained. Meanwhile, the fine camera's parameters are also determined from L–M optimization process. A flow chart of the proposed localization optimization method of 2-D control points for camera calibration algorithm is shown in Fig. 11.

V. Evaluation

It is difficult to judge whether the localization of control points are accurate using the image coordinate data of control points. Based on the fact that the more accurate localization of control points, the smaller the errors of the camera parameters, the proposed method is indirect evaluated by two assessment criterions. One is the traditional root mean square reprojection error E_1, which is usually for evaluate the camera calibration accuracy. It is computed by the Euclidean distance between the extracted 2-D control points $(x_{d,i}, y_{d,i})$ on the image and the reprojected point $(\tilde{x}_{d,i}, \tilde{y}_{d,i})$ from the corresponding point $M_{c,i}$ in 3-D space which projected onto the image plane through a calibrated camera model with lens distortion. The root mean square reprojection error E_1 can be defined as follows:

$$E_1 = \frac{1}{N} \sum_{i=1}^{N} \sqrt{(x_{d,i} - \tilde{x}_{d,i})^2 + (y_{d,i} - \tilde{y}_{d,i})^2}. \tag{23}$$

The second assessment criterion is the adjacent control points' distance deviation on the calibration plane. Once the camera has been calibrated, the 3-D position of the target plane can be obtained using calibrated parameters. Then, a 3-D projected point $M_{c,i} = (X_{d,i}, Y_{d,i}, Z_{d,i})$ can be determined by projecting the optical ray from the projection optical

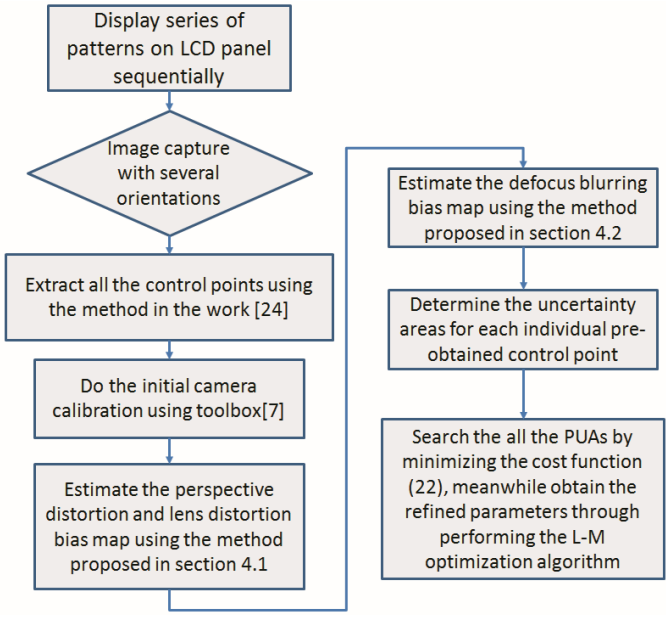

Fig. 11. Proposed localization optimization algorithm of 2-D control point for camera calibration.

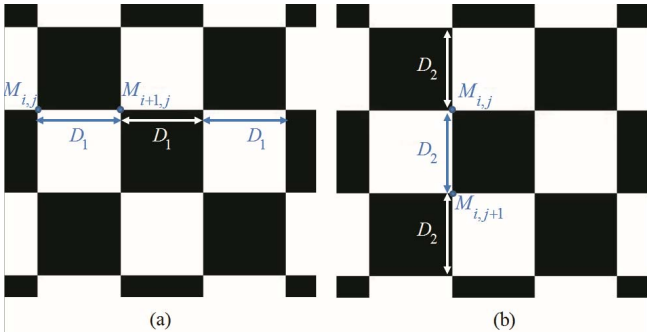

Fig. 12. Example (3×3 checkerboard pattern) of baseline Euclidean distance on target plane. (a) D_1. (b) D_2.

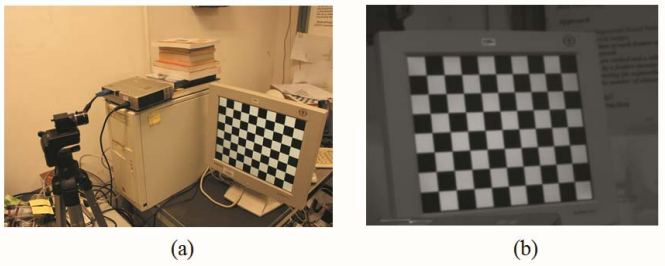

Fig. 13. (a) Experimental setup. (b) Sample image used for calibration.

center through the estimated control point intersecting with the known target plane. The assessment standard used in [30] is directly calculating the distance deviation between the observed 3-D test point test point $M_{c,i}$ and the projected point $\tilde{M}_{c,i}$, which is the interSection point on the target plane in 3-D space. However, comparing with obtaining the observed single testing point, it is much easier and more accurate to determine the relative distance in 3-D space. Therefore, in this paper, to assess the measurement result more accurately, we calculate two relative distances deviation on the real target plane between two adjacent 3-D points along with x-directional and y-directional, respectively, which are shown in Fig. 12. Given a $N_1 \times N_2$ checkerboard pattern image and the baseline value of the relative distance $D1$ and $D2$, which is the Euclidean distance of two adjacent 3-D spatial control points shown in Fig.12, the distance deviation E_{2x} and E_{2y} are given as follows:

$$E_{2x} = \frac{1}{N_1 * (N_2 + 1)} \sum_{i=1}^{N_1} \times \sum_{j=1}^{N_2+1} \sqrt{\left(\left\| \tilde{M}_{c,i,j} - \tilde{M}_{c,(i+1),j} \right\| - D_1 \right)^2} \quad (24)$$

$$E_{2y} = \frac{1}{(N_1 + 1) * N_2} \sum_{i=1}^{N_1+1} \times \sum_{j=1}^{N_2} \sqrt{\left(\left\| \tilde{M}_{c,i,j} - \tilde{M}_{c,i,(j+1)} \right\| - D_2 \right)^2}. \quad (25)$$

VI. Experimental Results

The proposed method is tested on the real-world and artificial scenarios. We conducted several experiments to assess the proposed method by evaluating the camera calibration accuracy and measurement accuracy. Fig. 13(a) shows the experimental setup in our work. A charge-coupled device camera (PointGray FL3-U3-13S2M-CS) is adopted for the experiments. It has the resolution of 1280 × 960 pixels.

The calibration target is a planar checkerboard pattern with 9 × 7 corner points (control points) evenly distributed on a LCD panel. The size of the pattern is 25 × 25 mm^2 and the benchmark distance between the adjacent points is 25 mm in both horizontal and vertical directions (in other words, $D_1 = D_2 = 25$ mm). One of the input images is shown in Fig. 13(b). We conduct three sets of experiments. In the first set of experiment, we intend to just simply demonstrate the out-of-focus blurring bias will decreases the camera calibration accuracy. And our proposed method and the conventional method implemented in [10] have been conducted to compare the calibration performance. To further compare the algorithm performance in calibration and measurement accuracy, real data with intentionally set defocus blurring and well-focused real data will be chosen in the second and the third set of experiment, respectively. It is worthy noticing that the assessment standard of calibration accuracy and measurement accuracy presented in Section V are used to evaluate the algorithm performance. In addition, variances of intrinsic parameters are also introduced to assess the results just in the first set of experiment.

A. Images With Artificial Blurring

In this experiment, we verify two important points. The first one is the fact that out-of-focus blurring decreases the camera calibration accuracy. In other word, the more out-of-focus blurring, the big error with control point's localization, thus less accuracy of camera's parameters. The second one is our proposed method is more robust than conventional

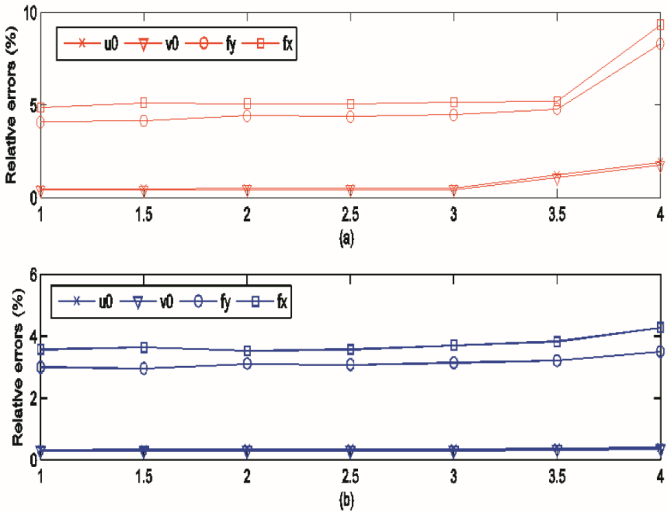

Fig. 14. (a) Relative variance of focal length (f_x, f_y) and principle point (u_0, v_0) using conventional method as blurring degree increases using conventional method. (b) Relative variance of focal length (f_x, f_y) and principle point (u_0, v_0) with the use of our proposed method as blurring degree increases using our proposed method.

method [10] even under the condition of out-of-focus blurring. A total of 18 images with different orientation are carefully taken for input data. It means that all the captured images of checkerboard pattern should be or can be supposed in-focus captured. After that, Gaussian kernels with different standard deviation ($\delta = 1, 1.5, 2, 2.5, 3, 3.5, 4$) are utilized to blur all precaptured in-focused images. Then, these blurred images are treated as input data for testing. As Fig. 14 shows, in general, with the defocus blurring becoming severer, the bigger relative variance of focal length and principle point increases with respect to the conventional method and the proposed method.

However, in Fig. 14(a), when using the conventional method, at the blur degree point where standard deviation of the Gaussian blurring kernel starts from 3, the relative variance of focal length becomes larger than using our proposed method which is shown in Fig. 14(b). Similarly, we can get the start point where blurring kernel equals 3.5, the relative coordinate variance of principle point using conventional method increases more sharply than using our proposed method. To further demonstrate the robustness in calibration accuracy when using our proposed method, we take another comparison analysis. In this comparison, one group of the most blurred previous captured image series data set is selected, which is the group with the biggest standard deviation of Gaussian blur kernel ($\delta = 4$). After corner extraction using conventional method and our proposed method, we obtain the calibrated parameters. The root mean square reprojection error with using of proposed method is 0.79659, while it is 1.398 with the use of conventional method. This result indicates that our proposed method outperforms than conventional method in the comparison of root mean square reprojection error. Hence, from the view of both the reprojection error and the relative variance of intrinsic parameters (f_x, f_y, u_0, v_0), our proposed method is more robust than the conventional method when a certain degree of out-of-focus blurring is introduced in the captured target images.

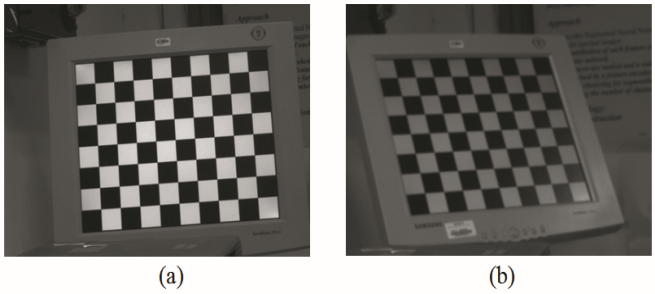

Fig. 15. Two sample images used for experiments. (a) Sample well-focused image for experiment 6.3. (b) Sample out-of-focused image for experiment 6.2.

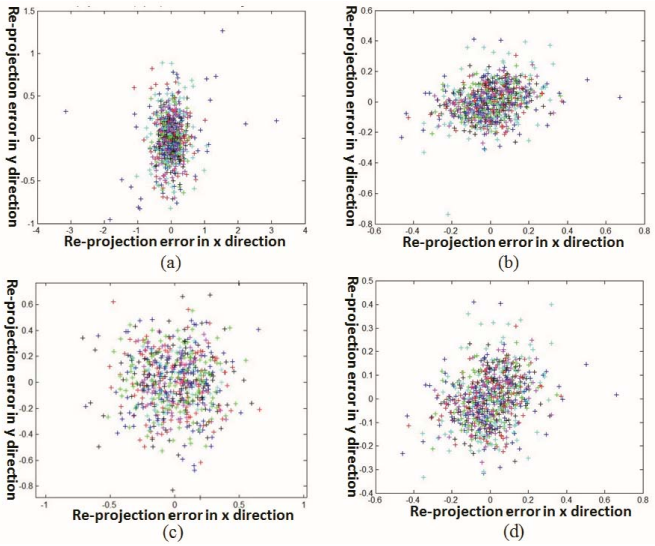

Fig. 16. Reprojection error analysis between four methods (unit:pixel). (a) Conventional method 1. (b) Conventional method 2. (c) Conventional method 3. (d) Our proposed method.

B. Real Data With Defocus Blurring

In this set of experiment, all the images are captured with intentionally out of focus setting to make the target plane with a certain degree of defocus. A total of 15 out-of-focus images were captured with different orientations. One of them is shown in Fig. 15(b).

Similar to the testing method in [30], 10 images are selected for calibration accuracy evaluation and five images are for measurement accuracy evaluation. The conventional method [10], which is selected as conventional method in Section VI-A, is denoted as method 1. More conventional methods, such as perspective distortion adjustment algorithm [24], a recently proposed corner extraction algorithm for camera calibration in [35], are additional adopted. They are denoted as method 2 and method 3, respectively. The quantitative results of reprojection error are given in Fig. 16. It is obvious that our proposed method shown in Fig. 16(d) presents a smaller reprojection error than the other three conventional methods. The quantitative calibrated accuracy results and the measurement accuracy results are also given in Tables I and II, respectively.

TABLE I
COMPARATIVE RESULTS OF CAMERA PARAMETERS AND CALIBRATION ACCURACY

	f_x (pixel)	f_y (pixel)	u_0 (pixel)	v_0 (pixel)	E_1 (pixel)
Method 1	4502.6811± 37.520	4505.9811± 33.114	656.4824± 59.729	498.8299± 40.707	0.63245
Method 2	4517.5157± 15.173	4520.0862± 13.338	659.9998± 24.591	510.6931± 21.039	0.24447
Method 3	4537.3553±33.225	4538.2280±29.522	596.7172±38.6635	523.6909±33.01856	0.3212
Our Method	4516.3017± 14.980	4519.1912± 13.166	657.1530± 24.139	514.2838± 20.837	0.2407

TABLE II
COMPARATIVE RESULTS OF MEASUREMENT ACCURACY

		Image 1	Image 2	Image 3	Image 4	Image 5	Average
Method 1	E_{2x} (mm)	0.0604	0.0521	0.0558	0.0545	0.0591	0.0564
	E_{2y} (mm)	0.0219	0.0466	0.0457	0.0476	0.0418	0.0407
Method 2	E_{2x} (mm)	0.0153	0.0256	0.0249	0.0314	0.0349	0.0264
	E_{2y} (mm)	0.0205	0.0229	0.0248	0.0268	0.0261	0.0242
Method 3	E_{2x} (mm)	0.03693	0.03656	0.04356	0.04134	0.04591	0.0409
	E_{2y} (mm)	0.03357	0.04937	0.04452	0.03371	0.03440	0.0391
Our method	E_{2x} (mm)	0.0144	0.0244	0.0235	0.0297	0.0335	0.0251
	E_{2y} (mm)	0.0200	0.0223	0.0235	0.0255	0.0233	0.0229

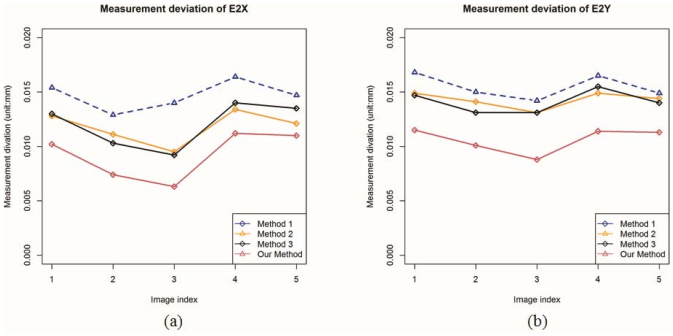

Fig. 17. Comparative results of measurement accuracy with respect to image index number. (a) E_{2x}. (b) E_{2y}.

As Table I shows, our proposed method outperforms than the method 1 with an impressive result about 62% less reprojection error, and meanwhile gives a less reprojection error comparing with conventional methods 2 and 3. The method 2, which uses perspective distortion adjustment, also presents a good performance on corner extraction accuracy even under some degree of defocus. The performance of method 3 is not so satisfactory due to its algorithm's presupposition is based on that the input images should be in-focus captured. However, it is still better than conventional method 1. Table II shows the comparative results of measurement accuracy. We can see that the average measurement error of five test images using our proposed method is $E_{2x} = 0.0251$ mm and $E_{2y} = 0.0229$ mm. It is the least measurement error comparing with the use of other three methods. For better observation of measurement accuracy, the measurement deviations (E_{2x} and E_{2y}) with respect to different test image (from image No. 1 to image No. 5) are shown in Fig. 17. We can clearly see that the proposed method outperforms than other three conventional methods with less measurement errors.

C. Practical and Generic Case

In this set of experiment, all the images are captured with carefully setting the target plane in-focus, which is the same as most of traditional work assumes. A total of 15 in-focus images were captured with different orientations. One of them is shown in Fig. 15(a). Similarly, we still use 10 images for calibration accuracy evaluation and five images for measurement accuracy evaluation. In this set of experiment, for better persuasive, method 1, method 2, and method 3 are still the same as in the previous experiment. The reprojection error figures are presented in Fig. 18.

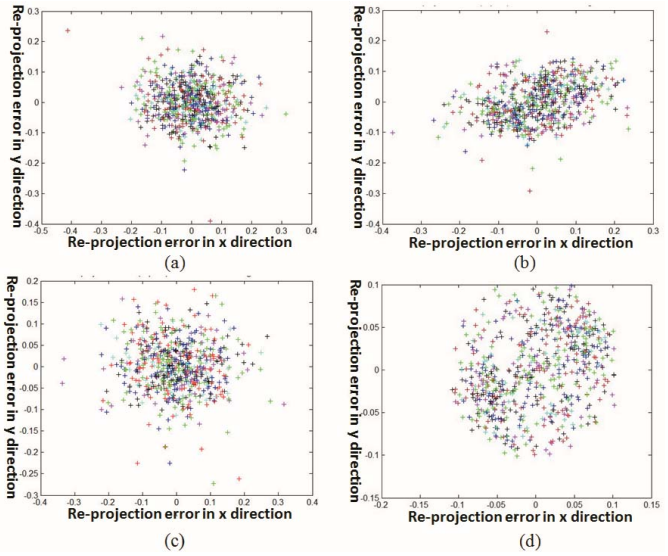

Fig. 18. Reprojection error analysis between four methods (unit:pixel). (a) Conventional method 1. (b) Conventional method 2. (c) Conventional method 3. (d) Our proposed method.

TABLE III
COMPARATIVE RESULTS OF CAMERA PARAMETERS AND CALIBRATION ACCURACY

Calibration technique	f_x (pixel)	f_y (pixel)	u_0 (pixel)	v_0 (pixel)	E_1 (pixel)
Method 1	4470.8328±12.3800	4473.3044±10.7004	677.48131±15.3026	512.7394±13.9629	0.15851
Method 2	4476.0392±12.9187	4477.1209±11.1639	674.61458±16.1596	510.9882±14.7038	0.15603
Method 3	4479.5903±12.5966	4480.97548±10.8738	683.44053±15.7001	509.40898±14.5237	0.1083
Our Method	4470.5607±8.2127	4471.1689±7.0951	686.50430±10.3449	517.2789±9.56745	0.0996

The detailed quantitative calibrated parameters and calibration accuracy results using different methods are given in Table III. The reprojection errors are 0.1581, 0.1560, and 0.1083 for conventional method 1, conventional method 2, and conventional method 3, respectively. It is worthy noticing that comparing with method 1, method 2 that uses perspective distortion adjustment based corner extraction algorithm, cannot improve the localization accuracy of control points much more when the input images are in-focus captured. And in these three conventional methods, the recently proposed conventional method 3 performs better than other two conventional methods. However, our proposed method outperforms than method 1, method 2, and method 3 with less reprojection error about 37%, 36%, and 8%, respectively. In the case of well-focused input images, our proposed optimal control point localization algorithm still gives the best calibration accuracy performance from the reprojection error perspective.

TABLE IV
COMPARATIVE RESULTS OF MEASUREMENT ACCURACY

		Image 1	Image 2	Image 3	Image 4	Image 5	Average
Method 1	E_{2x} (mm)	0.0154	0.0129	0.0140	0.0164	0.0147	0.0147
	E_{2y} (mm)	0.0168	0.0150	0.0142	0.0165	0.0149	0.0155
Method 2	E_{2x} (mm)	0.0128	0.0111	0.0095	0.0134	0.0121	0.0118
	E_{2y} (mm)	0.0149	0.0141	0.0131	0.0149	0.0144	0.0143
Method 3	E_{2x} (mm)	0.0130	0.0103	0.0092	0.0140	0.0135	0.0120
	E_{2y} (mm)	0.0147	0.0131	0.0131	0.0155	0.0140	0.0141
Our method	E_{2x} (mm)	0. 0102	0. 0074	0. 0063	0. 0112	0. 0110	0. 0092
	E_{2y} (mm)	0. 0115	0. 0101	0. 0088	0. 0114	0. 0113	0. 0106

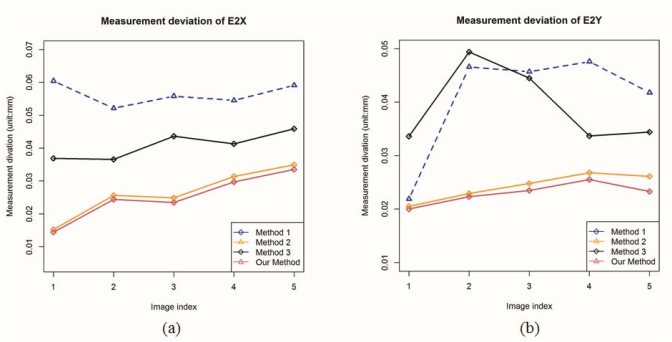

Fig. 19. Comparative results of measurement accuracy with respect to image index number. (a) E_{2x}. (b) E_{2y}.

To further demonstrate the robustness and outperformance of our proposed method, the detailed quantitative measurement accuracy results using four different techniques are given in Table IV. We can get the average measurement error using our proposed method is $E_{2x} = 0.\ 0092$ and $E_{2y} = 0.\ 0106$ mm. For better observation of measurement error, the measurement deviations (E_{2x} and E_{2y}) with respect to different test image (from image No. 1 to image No. 5) are shown in Fig. 19. Our proposed method outperforms than conventional method 1 and method 2 in measurement accuracy. We can clearly get that our proposed method outperforms than other three conventional methods with less measurement errors.

VII. DISCUSSION

Camera calibration plays an important role for many applications not only because it is indispensable for 3-D reconstruction and 3-D measurement in a stereovision system but also it reveals the properties of camera itself for manufacturing precise assessment. The motivation of this paper is to develop a generic method of 2-D control points' spatial localization optimization for robust and accurate camera calibration when the target plane is not in good focus condition. Our proposed alleviates the heavy dependence on subpixel corner extraction algorithm that is utilized for accurate control points' localization extraction. Once the optimal control points have been obtained, with existing camera model, the corresponding precise parameters can be easily determined. The proposed method is different from other control points determination methods from the latter, which are either by utilizing varies of complex corner extraction method or by iteratively perspective distortion correction, in that the latter needs more complicated algorithm or repetitive process to determine the precise localization of control point, yet may not be the ideal solution.

1) *Control PUA Estimation*: From the experiments, it is observed that the method of uncertainty area determination by introduce localization bias from defocus blurring, perspective distortion, and lens distortion is effective and valid. One could also simply take the whole blurring area for defocus blurring radius in PUA determination process. Some other factors, such as shadowing, uneven illumination, and other noises in input images could also be considered in the process of PUA determination. Theoretically, the more uncertainty control points contained in a PUA, the bigger chances of obtaining the optimal control points' localization. However, more uncertainty also means more complexity and time burden for searching the optimal solution will be heavier. Therefore, a balance has to be made for PUA determination. For a generic and practical case, taking control points' localization bias from defocus blurring, perspective distortion, and lens distortion using the proposed method in this paper is satisfactory.
2) *If Not Using Checkerboard Pattern*: In this paper, although we choose LCD panel displaying checkerboard pattern as calibration target, methods can also be developed in a similar way for treating other kinds of pattern when it is imaged under some degree of out of focus blurring. For example, in the case of circle array pattern or ring array pattern, the perspective distortion, and lens distortion bias map estimation can be easily performed in the same way. The uncertainty map from defocus blurring for circle center or the ring center can still be estimated using other image processing method. Hence, we then can determine the PUAs. Thus, in a similar way, the optimal localization for control points meanwhile with fine camera parameters can be obtained by searching the PUA.

VIII. CONCLUSION

This paper proposed a novel generic method of 2-D control point's spatial localization optimization for robust camera calibration. In the method, the optimal spatial localization of control points are estimated by searching the obtained PUAs, which are determined from defocusing blurring bias, perspective distortion, and lens distortion estimation. In the process of searching optimal control points, the final intrinsic parameters of camera are obtained by L–M optimization method at the same time. The GA for multivariables 2-D searching under constrain function of measurement accuracy enables high precision in the control points determination, thus further ensures camera calibration accuracy. The effectiveness and accuracy of the proposed method are verified through experiments using synthesized data and real images. In the future, we will apply the proposed method in a short baseline stereo system calibration to cope with the short baseline problem which actually is a bottleneck for short baseline stereovision systems. We will also apply it to the case of structured light system calibration under more practical conditions considering out-of-focus blurring.

REFERENCES

[1] R. Y. Tsai, "A versatile camera calibration technique for high-accuracy 3D machine vision metrology using off-the-shelf TV cameras and lenses," *IEEE J. Robot. Autom.*, vol. 3, no. 4, pp. 323–344, Aug. 1987.

[2] Z. Zhang, "A flexible new technique for camera calibration," *IEEE Trans. Pattern Anal. Mach. Intell.*, vol. 22, no. 11, pp. 1330–1334, Nov. 2000.

[3] V. Drenk, F. Hildebrand, M. Kindler, and D. Kliche, "A 3D video technique for analysis of swimming in a flume," in *Proc. 17th Int. Symp. Biomech. Sports Sci.*, 1999, pp. 361–364.

[4] H. Bacakoglu and M. S. Kamel, "A three-step camera calibration method," *IEEE Trans. Instrum. Meas.*, vol. 46, no. 5, pp. 1165–1172, Oct. 1997.

[5] O. D. Faugeras and G. Toscani, "The calibration problem for stereo," in *Proc. IEEE Conf. Comput. Vis. Pattern Recognit.*, Miami, FL, USA, 1986, pp. 15–20.

[6] W. Faig, "Calibration of close-range photogrammetry systems: Mathematical formulation," *Photogrammetric Eng. Remote Sens.*, vol. 41, no. 12, pp. 1479–1486, 1975.

[7] Y. I. Abdel-Aziz and H. M. Karara, "Direct linear transformation from comparator coordinates into object space coordinates in close-range photogrammetry," in *Proc. Amer. Soc. Photogrammetry Symp. Close-Range Photogrammetry*, Falls Church, VA, USA, 1971, pp. 1–18.

[8] C. A. Luna, M. Mazo, J. L. Lazaro, and J. F. Vazquez, "Calibration of line-scan cameras," *IEEE Trans. Instrum. Meas.*, vol. 59, no. 8, pp. 2185–2190, Aug. 2010.

[9] S. Y. Chen and Y. F. Li, "Self-recalibration of a color-encoded light system for automated 3-D measurements," *Meas. Sci. Technol.*, vol. 14, no. 1, pp. 33–40, 2003.

[10] J. Y. Bouguet. (2013, Oct. 10). *Camera Calibration Toolbox* [Online]. Available: http://www.vision.caltech.edu.bouguetj/calib_doc

[11] (2013, Oct. 10). *OpenCV* [Online]. Available: http://opencv.itseez.com/modules/calib3d/doc/calib3d.html

[12] K. Nakano, M. Okutomi, and Y. Hasegawa, "Camera calibration with precise extraction of feature points using projective transformation," in *Proc. IEEE ICRA*, May 2002, pp. 2532–2538.

[13] A. Datta, J.-S. Kim, and T. Kanade, "Accurate camera calibration using iterative refinement of control points," in *Proc. IEEE Conf. Comput. Vis. Workshops*, Sep./Oct. 2009, pp. 1201–1208.

[14] L. Lucchese and S. K. Mitra, "Using saddle points for subpixel feature detection in camera calibration targets," in *Proc. Asia-Pacific Conf. Circuits Syst.*, vol. 2. 2002, pp. 191–195.

[15] C. Harris and M. Stephens, "A combined corner and edge detector," in *Proc. Alvey Vis. Conf.*, 1988, pp. 147–151.

[16] J. L. L. Galilea, J.-M. Lavest, C. A. L. Vazquez, A. G. Vicente, and I. B. Munoz, "Calibration of a high-accuracy 3-D coordinate measurement sensor based on laser beam and CMOS camera," *IEEE Trans. Instrum. Meas.*, vol. 58, no. 9, pp. 3341–3346, Sep. 2009.

[17] S. Zhu and Y. Gao, "Noncontact 3-D coordinate measurement of cross-cutting feature points on the surface of a large-scale workpiece based on the machine vision method," *IEEE Trans. Instrum. Meas.*, vol. 59, no. 7, pp. 1874–1887, Jul. 2010.

[18] S. Chen and Y. F. Li, "Finding optimal focusing distance and edge blur distribution for weakly calibrated 3-D vision," *IEEE Trans. Ind. Inf.*, vol. 9, no. 3, pp. 1680–1687, Aug. 2013.

[19] Y. Li, Y. F. Li, Q. L. Wang, D. Xu, and M. Tan, "Measurement and defect detection of the weld bead based on online vision inspection," *IEEE Trans. Instrum. Meas.*, vol. 59, no. 7, pp. 1841–1859, Jul. 2010.

[20] F. Shu, L. Toma, W. Neddermeyer, and J. Zhang, "Precise online camera calibration in a robot navigating vision system," in *Proc. IEEE Int. Conf. Mechatron. Autom.*, vol. 3. Niagara Falls, ON, Canada, 2005, pp. 1277–1282.

[21] M. Baba, M. Mukunoki, and N. Asada, "A unified camera calibration using geometry and blur of feature points," in *Proc. 18th ICPR*, vol. 1. 2006, pp. 816–819.

[22] D. Scaramuzza, A. Martinelli, and R. Siegwart, "A flexible technique for accurate omnidirectional camera calibration and structure from motion," in *Proc. IEEE ICVS*, Jan. 2006, p. 45.

[23] C. Mei and P. Rives, "Single view point omnidirectional camera calibration from planar grids," in *Proc. IEEE Int. Conf. Robot. Autom.*, Apr. 2007, pp. 3945–3950.

[24] M. Higuchi. (2013, Oct. 10). *Software Package for Precise Camera Calibration* [Online]. Available: http://www.ri.cmu.edu/research_project_detail.html?project_id=617&menu_id=261

[25] S. Zhuo and T. Sim, "Defocus map estimation from a single image," *Pattern Recognit.*, vol. 44, no. 9, pp. 1852–1858, 2011.

[26] P. Favaro and S. Soatto, "A geometric approach to shape from defocus," *IEEE Trans. Pattern Anal. Mach. Intell.*, vol. 27, no. 3, pp. 406–417, Mar. 2005.

[27] S. Douxchamps and K. Chihara, "High-accuracy and robust localization of large control markers for geometric camera calibration," *IEEE Trans. Pattern Anal. Mach. Intell.*, vol. 31, no. 2, pp. 376–383, Feb. 2009.

[28] Z. Song and R. Chung, "Use of LCD panel for calibrating structured-light-based range sensing system," *IEEE Trans. Instrum. Meas.*, vol. 57, no. 11, pp. 2623–2630, Nov. 2008.

[29] S. Y. Chen and Y. F. Li, "Determination of stripe edge blurring for depth sensing," *IEEE Sensors J.*, vol. 11, no. 2, pp. 389–390, Feb. 2011.

[30] F. Zhou, Y. Cui, Y. Wang, L. Liu, and H. Gao, "Accurate and robust estimation of camera parameters using RANSAC," *Opt. Lasers Eng.*, vol. 51, no. 3, pp. 197–212, 2013.

[31] Q. Ji and Y. Zhang, "Camera calibration with genetic algorithms," *IEEE Trans. Syst., Man, Cybern. A, Syst., Humans*, vol. 31, no. 2, pp. 120–130, Mar. 2001.

[32] S. Hati and S. Sengupta, "Robust camera parameter estimation using genetic algorithm," *Pattern Recognit. Lett.*, vol. 22, nos. 3–4, pp. 289–298, 2001.

[33] C. C. Balascio, D. J. Palmeri, and H. Gao, "Use of a genetic algorithm and multi-objective programming for calibration of a hydrologic model," *Trans. ASAE*, vol. 41, no. 3, pp. 615–619, 1998.

[34] M. Melanie, *An Introduction to Genetic Algorithms*. Cambridge, MA, USA: MIT Press, 1998.

[35] A. Geiger, F. Moosmann, O. Car, and B. Schuster, "Automatic camera and range sensor calibration using a single shot," in *Proc. IEEE ICRA*, May 2012, pp. 3936–3943.

Jianyang Liu received the B.S. and M.S. degrees from the Department of Applied Physics, Sichuan University, Chengdu, China, in 2008 and 2011, respectively. He is currently pursuing the Ph.D. degree with the Department of Mechanical and Biomedical Engineering, City University of Hong Kong, Hong Kong.

His current research interests include computer vision, robotics, 3-D metrology, and image analysis.

Youfu Li received the Ph.D. degree in robotics from the Department of Engineering Science, University of Oxford, Oxford, U.K., in 1993.

He was a Post-Doctoral Research Associate with the Department of Computer Science, University of Wales, Cardiff, U.K., from 1993 to 1995. He joined the City University of Hong Kong, Hong Kong, in 1995, where he is currently a Professor with the Department of Mechanical and Biomedical Engineering. His current research interests include robot vision, visual tracking, sensing, and sensor-based control for robotics.

Prof. Li has served as an Associate Editor of the IEEE TRANSACTIONS ON AUTOMATION SCIENCE AND ENGINEERING, and is currently serving as the Guest Editor of the IEEE ROBOTICS AND AUTOMATION MAGAZINE and an Editor of the IEEE Robotics Automation Society's Conference Editorial Board.

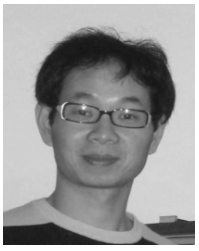

Shengyong Chen (M'01–SM'10) received the Ph.D. degree in computer vision from the City University of Hong Kong, Hong Kong, in 2003.

He joined the Zhejiang University of Technology, Hangzhou, China, in 2004, where he is currently a Professor with the Department of Computer Science. He was with the University of Hamburg, Hamburg, Germany, from 2006 to 2007. He was a Visiting Professor at Imperial College, London, U.K., from 2008 to 2009, and the University of Cambridge, Cambridge, U.K., in 2012. He has authored over 100 scientific papers in international journals and conferences. His current research interests include computer vision, robotics, 3-D object modeling, and image analysis.

Dr. Chen is a fellow of the Institution of Engineering and Technology (IET) and a committee member of the IET Shanghai Branch. He was a recipient of the Fellowship from the Alexander von Humboldt Foundation of Germany.